

Numerical Simulation of Heat and Mass transfer in Stagnation point flow of Casson Nanofluid over a Porous Stretching sheet with Thermal Radiation.

Kapil kumar^{1,*}, Bhupander Singh¹, Pravendra Kumar¹, Rahul Kumar¹

¹ Department of Mathematics, Meerut College, Meerut, U.P.-250002

Abstract

This study presents the heat and mass transfer analysis in stagnation point flow of MHD Casson nanofluid over a stretching sheet with thermal radiation effect in porous medium. The set of non-linear partial differential equations (PDEs) leading the study of fluid flow are transformed into a system of ordinary differential equations (ODEs) using similarity transformations and non-dimensional variables, which are then numerically solved by the `bvp4c` built-in MATLAB software. The impact of pertinent parameters like Casson fluid parameter, porosity parameter, magnetic parameter, stagnation point parameter, thermal radiation parameter, Prandtl number, Brownian motion parameter, thermophoresis parameter and Lewis number on velocity, temperature, and concentration profiles is graphically shown and discussed.

Keywords: Nanofluid, Casson fluid, Stretching sheet, Magneto hydrodynamics, Thermal Radiation, Porous medium

1. Introduction

A fundamental problem in fluid dynamics is the boundary layer flow analysis of viscous incompressible fluids across a stretched sheet owing to stagnation point flow. The study of two-dimensional fluid flow at a stagnation point across a surface was first done by Hiemenz [1]. Later, the issue of stagnation point flow was expanded in a number of ways to take different fluid types and physical effects into account. The practical applications in industry and industrial processing have drawn a lot of interest to the study of boundary layer stagnation point flow over a surface extended to non-Newtonian fluids. Practical applications include, but are not limited to, the polymer processing industries; biological processes; environmental pollution; aerodynamic plastic sheet extrusion; glass fiber production of the boundary layer along a liquid film; condensation process; and the cooling and/or drying of paper and textiles. Furthermore, metallurgical processes and petroleum production are only two examples of the many industrial applications where heat transfer analysis of non-Newtonian fluids is crucial. Sakiadis [2] was the first to study boundary layer flow resulting from a stretching sheet on a continually stretching surface moving at a constant speed. Tsou et al.'s experimentation [3] expanded on his findings by examining the flow of heat transfer in the boundary layer on a constantly moving surface.

Magneto hydrodynamic (MHD) flow is an extremely important field of study because many industrial processes, including the processing of magnetic materials, the purification of crude oil, the production of MHD electrical power, the manufacturing of glass, geophysics, and paper, depend on the influence of a

magnetic field on the viscous flow of an electrically conducting fluid. Ghazwani et al. [4] have studied the application of nanoparticles in magneto hydrodynamics (MHD) stagnation point flow across a stretchy surface with porosity effect and boundary slip phenomena. Taking into account a number of variables, including thermal radiation, changeable fluid viscosity, Joule heating, and viscous dissipation, Ali et al. [5] examined MHD nanofluid flow across a non-linear stretchable surface in the presence of an electric field. In order to examine the effects of a magnetic field, thermal radiation, and chemical reaction on the flow and heat transfer of boundary layer in nanofluids over a non-isothermal stretching surface via a permeable porous media, Awati et al. [6] conducted an analysis. Waqas et al.'s [7] three-dimensional study of the mass and heat transfer characteristics of a hybrid nanofluid, along with electro-magneto hydrodynamics, was aimed at improving heat transmission. Viscosity dissipation of an exponentially extending sheet and internal heat production in Casson MHD nanofluid flow were explored numerically by Kemparaju et al. [8].

Common fluids like water and ethylene glycol, for example, have their thermal conductivity improved by mixing metal or metallic oxide nanoparticles with a base fluid to speed up heat transfer by improving the nanofluid's thermal transport. This can be attributed to the nanoparticles' increased heat conductivity and the corresponding Brownian motion. Nanofluids are stable suspensions of nanoparticles in base fluids, which exhibit improved thermophysical properties compared to the base fluid alone [9]. Nanofluids have been used in various industries, including solar panels and CO₂ absorption [10]. In the oil and gas industry, nano-emulsions with adjustable density have been used as cleaning fluids to remove sludge from well walls [11]. The addition of nanoparticles to fluids creates smart flu-

*Corresponding author

Email address: kapiltomadia071993@gmail.com (Kapil kumar)

ids, which have enhanced properties that depend on nanoparticle dimensions. These nanofluids have advantages such as increased sedimentation stability and improved thermal, optical, stress-strain, electrical, and rheological properties. Thermal radiation has been investigated in several papers. The effect of thermal radiation on the flow of nanofluid and heat transfer over a porous stretching/shrinking surface under the influence of an angled magnetic field was investigated by Fu Gui et al. [12]. The impact of a magnetic field on unsteady magnetohydrodynamic (MHD) water-based nanofluid flow with radiative heat transfer was examined by Reddy et al. [13]. The impact of heat radiation on the three-dimensional magnetized rotating flow of a hybrid nanofluid was studied statistically by Asghar et al. [14]. In the presence of copper nanoparticles and gyrotactic bacteria, Bhupendra K. et al. [15] investigated the effects of mass transfer, heat transmission, and entropy formation on the flow of Jeffrey fluid under the influence of solar light. Neha et al. [16] computationally investigated the thermally radiative incompressible flow of hybrid nanofluid induced by a radially stretchable rotating disk.

Casson nanofluid is a type of nanofluid that has been extensively studied in various research papers. It is known for its excellent heat transfer rates and has numerous applications in medical and industrial fields [17]. The behavior of Casson nanofluid has been investigated in different scenarios, such as in a porous medium [18], in the presence of swimming motile organisms [19], and under the influence of an applied changing magnetic flux [20]. Mathematical models and numerical methods have been used to analyze the flow and thermal/mass transfer characteristics of Casson nanofluid [21]. The effects of various parameters, such as viscosity, conductivity, Darcy parameter, and magnetic field, have been studied to understand the behavior of Casson nanofluid. Overall, the research on Casson nanofluid provides valuable insights into its properties and potential applications in different fields.

2. Problem Formulation

In the current mathematical model, we consider two-dimensional steady MHD state stagnation point flow of Casson nanofluid across a stretching sheet in porous medium. The coordinate system is set up in a way that the x-axis is along the sheet's surface, while the y-axis is oriented perpendicular to the sheet. Moreover, the flow occurs in the region where $y \geq 0$. As y tends to infinity, the ambient values of T and C are represented by T_∞ and C_∞ , respectively. The distribution of the free-stream velocity is assumed to follow the form of $U_\infty = ax$, where $u_w = bx$ represents the velocity of the stretching sheet, with a and b being positive constants. The steady, laminar boundary layer flow equations for a Casson nanofluid passing over a stretching sheet, along with the boundary layer approximation, encompass expressions for mass, momentum, thermal energy, and concentration.

$$\frac{\partial u}{\partial x} + \frac{\partial v}{\partial y} = 0 \quad (1)$$

$$u \frac{\partial u}{\partial x} + v \frac{\partial v}{\partial y} = U_\infty \frac{\partial U_\infty}{\partial x} + \nu \left(1 + \frac{1}{\beta} \right) \frac{\partial^2 u}{\partial y^2} - \frac{\nu}{\kappa_1} (u - U_\infty) - \frac{\sigma B_0^2}{\rho} (u - U_\infty) \quad (2)$$

$$u \frac{\partial T}{\partial x} + v \frac{\partial T}{\partial y} = \alpha \frac{\partial^2 T}{\partial y^2} + \frac{(\rho C_p)_p}{(\rho C_p)_f} \left[D_B \frac{\partial T}{\partial y} \frac{\partial C}{\partial y} + \frac{D_T}{T_\infty} \left(\frac{\partial T}{\partial y} \right)^2 \right] - \frac{1}{\rho C_p} \frac{\partial q_r}{\partial y} \quad (3)$$

$$u \frac{\partial C}{\partial x} + v \frac{\partial C}{\partial y} = D_B \frac{\partial^2 C}{\partial y^2} + \frac{D_T}{T_\infty} \frac{\partial^2 T}{\partial y^2} \quad (4)$$

The specific boundary conditions for the problem are outlined as follows:

$$u = u_w = bx, \quad v = 0, \quad T = T_w, \quad C = C_w \quad \text{at } y = 0 \quad (5)$$

$$u = U_\infty = ax, \quad C = C_\infty, \quad T = T_\infty \quad \text{as } y \rightarrow \infty \quad (6)$$

The quantities u and v represent the velocity components of the Jeffrey nanofluid in the x and y directions, respectively. In the energy boundary layer equation (3), the radiative heat flux q_r is estimated using the Rosseland approximation [22] for thermal radiation, which is expressed as follows:

$$q_r = -\frac{4}{3} \frac{\sigma^*}{k^*} \frac{\partial T^4}{\partial y} \quad (7)$$

Whereas σ^* = Stephan Boltzmann constant, k^* = Rosseland mean spectral absorption coefficient.

Through a Taylor series expansion centered at the ambient temperature T_∞ , it becomes apparent that the term T^4 can be treated as a linear relationship with temperature. This simplification is attained by disregarding higher-order terms in the approximation process.

$$T^4 \approx 4T_\infty^3 T - 3T_\infty^4 \quad (8)$$

Utilizing Equations (7) and (8), we derive the following:

$$\frac{\partial q_r}{\partial y} = -\frac{16}{3} \frac{\sigma^* T_\infty^3}{k^*} \frac{\partial^2 T}{\partial y^2} \quad (9)$$

The analysis of the problem is made simpler by introducing the following similarity transformation:

$$\psi = \sqrt{b\nu x} f(\eta), \quad \eta = y \sqrt{\frac{b}{\nu}}$$

$$\theta(\eta) = \frac{T - T_\infty}{T_f - T_\infty}, \quad \phi(\eta) = \frac{C - C_\infty}{C_\infty} \quad (10)$$

where $\psi(x, y)$ represent the stream function and is defined as,

$$u = \frac{\partial \psi}{\partial y}, \quad v = -\frac{\partial \psi}{\partial x} \quad (11)$$

Equations (1) satisfy identically and equations (2), (3), and (4) are reduced to the following set of nonlinear ODE's with the help of the similarity transformation described above.

$$\left(1 + \frac{1}{\beta}\right) f''''(\eta) - (f'(\eta))^2 + f(\eta)f''(\eta) + (M + K)(r - f'(\eta)) + r^2 = 0 \quad (12)$$

$$(1 + Nr)\theta''(\eta) + Pr[\theta'(\eta)f(\eta) + N_b\theta'(\eta)\phi'(\eta) + N_t(\theta'(\eta))^2] = 0 \quad (13)$$

$$\phi''(\eta) + LePrf(\eta)\phi'(\eta) + \frac{N_t}{N_b}\theta''(\eta) = 0 \quad (14)$$

using the appropriate boundary condition as determined by Eqs. (5) and (6) in the form:

$$f(0) = 0, f'(0) = 1, \theta(0) = 1, \phi(0) = 1 \quad \text{at } \eta = 0 \quad (15)$$

$$f'(\eta) = r, \theta(\eta) = 0, \phi(\eta) = 0 \quad \text{at } \eta \rightarrow \infty \quad (16)$$

The Brownian motion parameter, the thermophoresis parameter, the thermal radiation parameter, the Prandtl number, Hartmann number, the porosity parameter, stagnation point parameter and the Lewis number are represented by the similarity parameters N_b , N_t , Nr , Pr , β , K , M , r and Le respectively in the equations mentioned above (12)-(16). They are defined as follows:

$$N_b = \frac{\Gamma D_B C_\infty}{\nu}, N_t = \frac{\Gamma D_T}{\nu T_\infty}(T_f - T_\infty), Nr = \frac{16 \sigma^* T_\infty^3}{3 K^* K_f},$$

$$Pr = \frac{\nu}{\alpha}, M = \frac{\sigma B_0^2}{b \rho}, K = \frac{\nu}{b k_1}, r = \frac{a}{b}, Le = \frac{\alpha}{D_B} \quad (17)$$

Quantities like the rate of mass and heat transfer, as well as coefficient of friction factor, are interpreted as follows:

$$C_f = \frac{2 \tau_w}{\rho u_w^2}, Nu_x = \frac{x q_w}{k_f(T_w - T_\infty)}, Sh_x = \frac{x q_m}{D_B(C_w - C_\infty)} \quad (18)$$

Where τ_w denote wall shear stress, surface heat flux is q_w and q_m shows mass flux.

$$\sqrt{Re_x} C_f = \left(1 + \frac{1}{\beta}\right) f''(0), \frac{Nu_x}{\sqrt{Re_x}} = -(1 + Nr)\theta'(0),$$

$$\frac{Sh_x}{\sqrt{Re_x}} = -\phi'(0) \quad (19)$$

3. Solution Algorithm:

The MATLAB bvp4c technique is applied to numerically solve the equations described above. Equations (12), (13), and (14) are converted into first-order differential equations, and then solved while adhering to the specified boundary conditions (15)-(16) to interface with the bvp4c solver. The resulting set

of first-order differential equations, along with the transformed boundary conditions (20)-(28), is as follows:

$$f = y_1, f' = y_2, f'' = y_3, \theta = y_4, \theta' = y_5, \phi = y_6, \phi' = y_7 \quad (20)$$

Equations (10), (11), (12), (13) and (14) become

$$y_1' = y_2 \quad (21)$$

$$y_2' = y_3 \quad (22)$$

$$y_3' = \frac{1}{(1 + 1/\beta)} [y_2^2 - r^2 - y_1 y_3 - (M + K)(r - y_2)] \quad (23)$$

$$y_4' = y_5 \quad (24)$$

$$y_5' = -\frac{Pr}{(1 + Nr)} [y_1 y_5 + N_b y_5 y_7 + N_t y_5^2] \quad (25)$$

$$y_6' = y_7 \quad (26)$$

$$y_7' = -LePr y_1 y_7 + \frac{N_t Pr}{N_b(1 + Nr)} [y_1 y_5 + N_b y_5 y_7 + N_t y_5^2] \quad (27)$$

The boundary condition yields

$$y_1(0) = 0, y_2(0) = 1, y_4(0) = 1, y_6(0) = 1 \quad \text{at } \eta \rightarrow 0$$

$$y_2(\eta) = r, y_4(\eta) = 0, y_6(\eta) = 0 \quad \text{at } \eta \rightarrow \infty \quad (28)$$

4. Results and discussion:

Under the boundary conditions (15) and (16), the reduced nonlinear ordinary differential equations (12)–(14) are numerically solved using the Bvp4c method. Several values of the physical parameters are tested for this numerical solution. The impact of changing the governing parameters on the skin friction coefficient, concentration, temperature, dimensionless velocity, and local heat and mass transfer rates is investigated.

Table 1: Effect of various parameter on skin friction coefficient C_f

β	K	M	r	$f''(0)$	$(1 + 1/\beta)f''(0)$
0.5	0.6	1	0.5	- 0.5299	- 1.5897
1	0.6	1	0.5	- 0.6487	- 1.9461
1.5	0.6	1	0.5	- 0.7106	- 2.1318
2.0	0.6	1	0.5	- 0.7490	- 2.2470
1	0.5	1	0.5	- 0.6391	- 1.7042
1	1.0	1	0.5	- 0.6860	- 1.8293
1	1.5	1	0.5	- 0.7300	- 1.9466
1	2.0	1	0.5	- 0.7715	- 2.0573
1	0.6	0.5	0.5	- 0.5989	- 1.1978
1	0.6	1.0	0.5	- 0.6487	- 1.2974
1	0.6	1.5	0.5	- 0.6950	- 1.3900
1	0.6	2.0	0.5	- 0.7385	- 1.4770
1	0.6	1	0.1	- 1.0564	- 2.1128
1	0.6	1	0.2	- 0.9647	- 1.9294
1	0.6	1	0.3	- 0.8660	- 1.7320
1	0.6	1	0.4	- 0.7606	- 1.5212

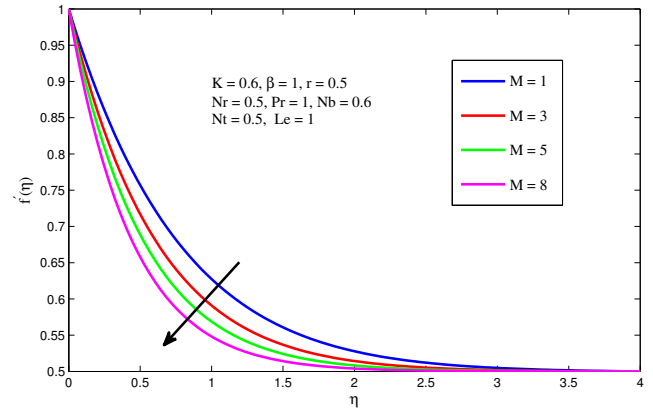


Figure 2: Effect of Magnetic parameter on velocity of the fluid.

Figure 2 illustrates how raising the magnetic field parameter has a negative impact on the velocity profile. The Lorentz force is created as a result of the rising magnetic field's strengthening of the external electric field. In the opposite direction of the flow, the Lorentz force acts on the surface to lower velocity.

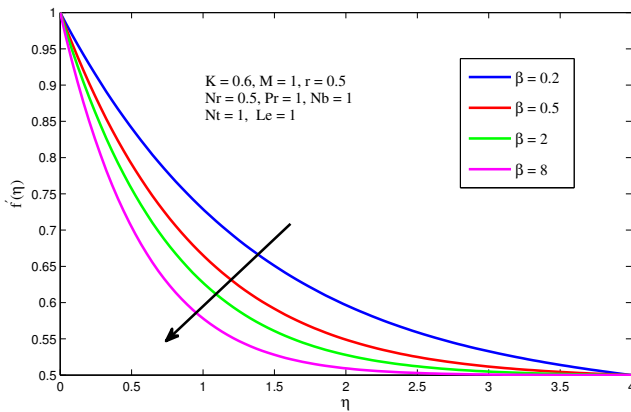


Figure 1: Effect of Casson fluid parameter on velocity of the fluid.

The velocity graph's fluctuation in relation to the Casson parameter β is shown in Fig. 1. The graph indicates that the velocity boundary layer thickness reduces as the values of β grow. This is because a rise in β causes a rise in plastic dynamic viscosity, which creates resistance to fluid flow and results in a drop in fluid velocity.

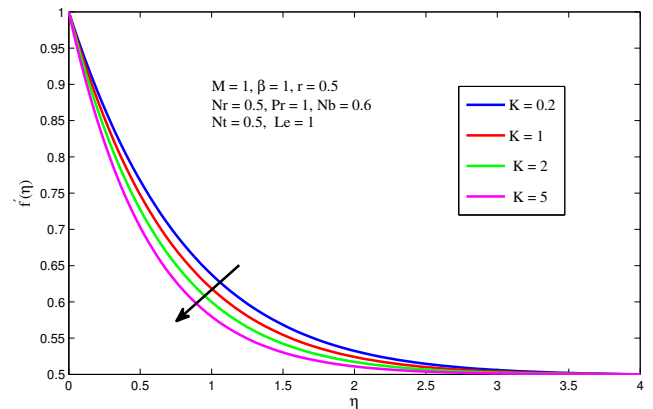


Figure 3: Effect of Porosity parameter on velocity of the fluid.

As can be seen in Fig. 3 the velocity profile decreases as the porosity parameter varies. It indicates that as pores are bigger, the momentum of the flow across the boundary layer gets less. Additionally, the presence of a porous medium raises flow resistance, which lowers fluid motion and, as a result, lowers nanofluid velocity.

Table 2: The variation of Nusselt number (Nu_x) and Sherwood number (Sh_x) with respect to different parameters.

β	K	M	r	Nr	Pr	N_b	N_t	Le	$-(1+Nr)\theta'(0)$	$-\phi'(0)$
0.5	0.6	1	0.5	0.5	1	0.6	0.5	1	0.6461	0.6028
1	0.6	1	0.5	0.5	1	0.6	0.5	1	0.6284	0.5927
1.5	0.6	1	0.5	0.5	1	0.6	0.5	1	0.6230	0.5883
2.0	0.6	1	0.5	0.5	1	0.6	0.5	1	0.6200	0.5857
1	0.5	1	0.5	0.5	1	0.6	0.5	1	0.6292	0.5934
1	1.0	1	0.5	0.5	1	0.6	0.5	1	0.6254	0.5902
1	1.5	1	0.5	0.5	1	0.6	0.5	1	0.6219	0.5874
1	2.0	1	0.5	0.5	1	0.6	0.5	1	0.6188	0.5849
1	0.6	0.5	0.5	0.5	1	0.6	0.5	1	0.6326	0.5964
1	0.6	1.0	0.5	0.5	1	0.6	0.5	1	0.6284	0.5927
1	0.6	1.5	0.5	0.5	1	0.6	0.5	1	0.6246	0.5896
1	0.6	2.0	0.5	0.5	1	0.6	0.5	1	0.6212	0.5869
1	0.6	1	0.5	0.5	1	0.6	0.5	1	0.6284	0.5927
1	0.6	1	1.0	0.5	1	0.6	0.5	1	0.7278	0.6878
1	0.6	1	1.5	0.5	1	0.6	0.5	1	0.8139	0.7740
1	0.6	1	2.0	0.5	1	0.6	0.5	1	0.8904	0.8509
1	0.6	1	0.5	0.5	1	0.6	0.5	1	0.5892	0.5927
1	0.6	1	0.5	1.0	1	0.6	0.5	1	0.7340	0.6089
1	0.6	1	0.5	1.5	1	0.6	0.5	1	0.8710	0.6215
1	0.6	1	0.5	2.0	1	0.6	0.5	1	1.0038	0.6312
1	0.6	1	0.5	0.5	0.5	0.6	0.5	1	0.5481	0.4100
1	0.5	1	0.5	0.5	1.0	0.6	0.5	1	0.6284	0.5927
1	0.6	1	0.5	0.5	1.3	0.6	0.5	1	0.6457	0.7053
1	0.6	1	0.5	0.5	1.5	0.6	0.5	1	0.6472	0.7797
1	0.6	1	0.5	0.5	1	0.5	0.5	1	0.6544	0.5581
1	0.6	1	0.5	0.5	1	1.0	0.5	1	0.5323	0.6597
1	0.6	1	0.5	0.5	1	1.5	0.5	1	0.4291	0.6899
1	0.6	1	0.5	0.5	1	2.0	0.5	1	0.3430	0.7027
1	0.6	1	0.5	0.5	1	0.6	1.0	1	0.5536	0.5500
1	0.6	1	0.5	0.5	1	0.6	1.5	1	0.4881	0.5576
1	0.6	1	0.5	0.5	1	0.6	2.0	1	0.4305	0.6063
1	0.6	1	0.5	0.5	1	0.6	2.5	1	0.3798	0.6891
1	0.6	1	0.5	0.5	1	0.6	0.5	1	0.6633	0.3539
1	0.6	1	0.5	0.5	1	0.6	0.5	1	0.6284	0.5927
1	0.6	1	0.5	0.5	1	0.6	0.5	1	0.6078	0.7867
1	0.6	1	0.5	0.5	1	0.6	0.5	1	0.5945	0.9499

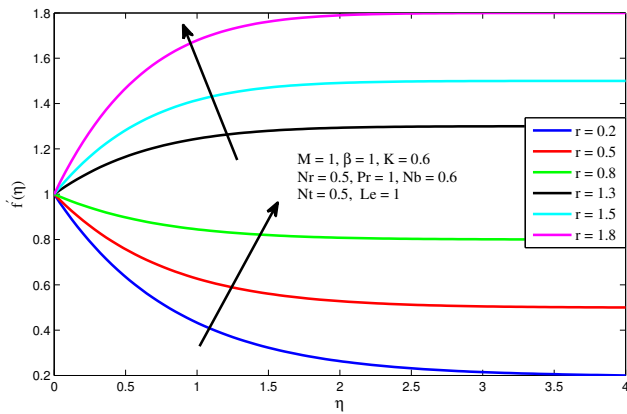


Figure 4: Effect of Stagnation point parameter on velocity of the fluid.

The impact of velocity ratio parameter r on the velocity graph is seen in Fig. 4. The flow velocity increases when the free-stream velocity surpasses the stretching sheet's velocity, or when $r \geq 1$. Nevertheless, the thickness of the boundary layer decreases as r increases. Moreover, the velocity graph approaches the velocity ratio parameter r when the free-stream velocity is higher than the stretching velocity. On the other hand, there is a drop in fluid velocity and hydrodynamic boundary layer thickness when the free-stream velocity is smaller than the stretching sheet velocity.

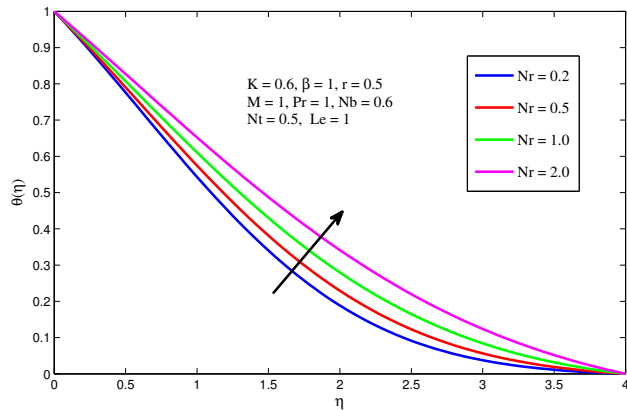


Figure 5: Effect of Radiation parameter on velocity of the fluid.

The analysis of Fig. 5 shows that raising the value of Rd raises the temperature profile. The heat transfer rate inside the boundary layer area is increased by a larger value of Rd because it transfers more heat to the working fluid between the two layers.

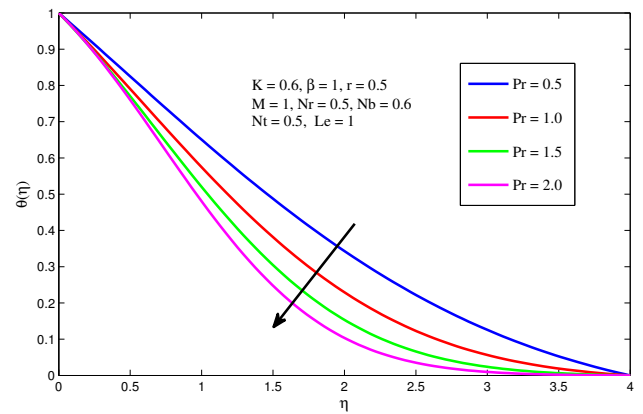


Figure 6: Effect of Prandtl number on temperature of the fluid.

The temperature profile changes when the Prandtl number is applied, as seen in Fig. 6. The Prandtl number is the momentum diffusivity divided by the thermal diffusivity. A lower amount of thermal diffusivity is associated with an increase in Prandtl number. Therefore, the temperature drops due to a decrease in thermal diffusion.

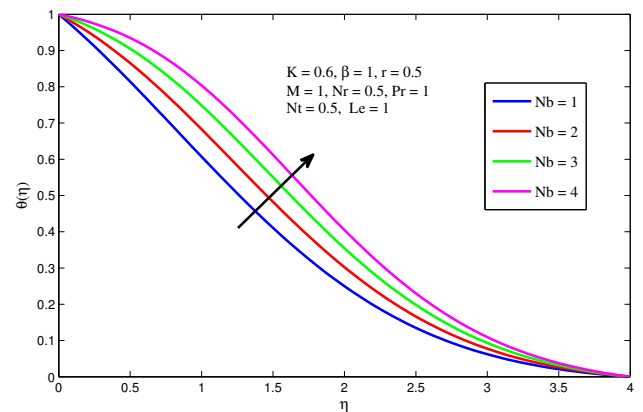


Figure 7: Effect of Brownian motion parameter on temperature of the fluid.

The influence of N_b on the temperature profile is displayed in Figure 7. It is evident that when N_b rises, mass diffusivity increases as well, raising the temperature in the boundary layer segment.

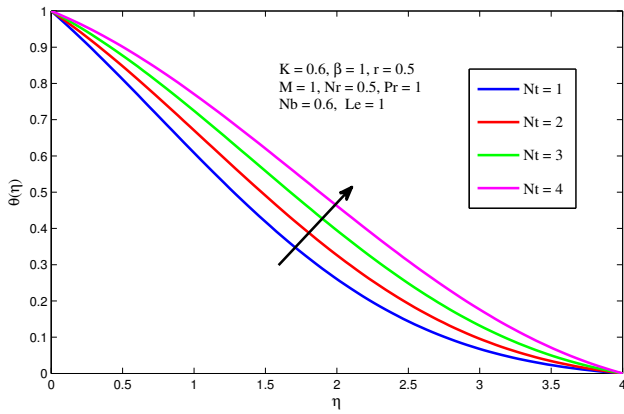


Figure 8: Effect of thermophoresis parameter on temperature of the fluid.

The plotted impacts of N_t on the temperature profile is shown in Fig. 8. It is evident that when N_t rises, the temperature profile rises as well. It occurs as a result of the increased thermophoresis force caused by higher values of N_t , which has the propensity to transfer nanoparticles from hot surfaces to cold surfaces. Consequently, heat transmission rates for nanoparticles increase in the boundary layer area.

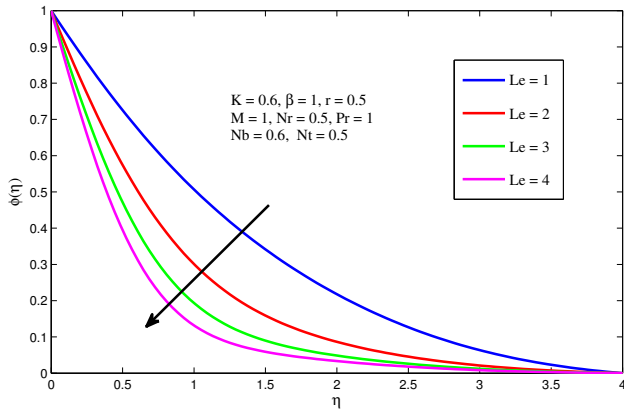


Figure 9: Effect of Lewis number on Concentration profile.

The effect of the Lewis number on the nanoparticle concentration profile is seen in Fig. 9. Higher values of Lewis number Le , which is correlated with nanoparticle concentration and reduces mass concentration with the base fluid and nanoparticles, are evident as the Lewis number is the ratio of heat diffusivity to mass diffusivity. As a result, the value of Le increases and the concentration profile of nanoparticles lowers.

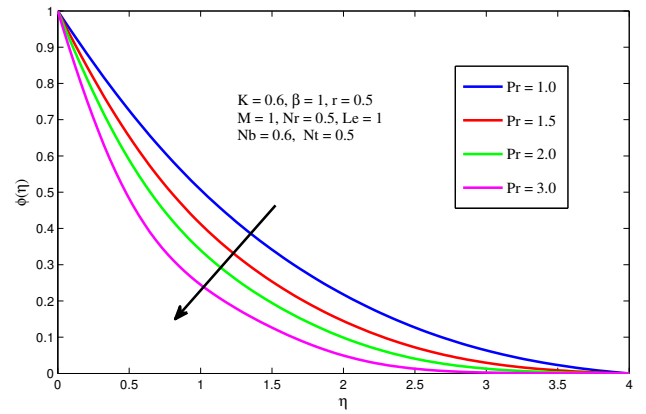


Figure 10: Effect of Prandtl number on Concentration profile.

The similar consequences was observed from the Fig.10 with the parameter Pr .

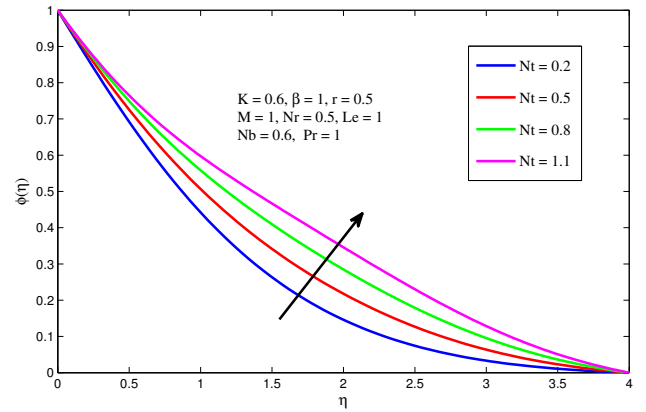


Figure 11: Effect of thermophoresis parameter on Concentration profile.

The effects of nanoparticle concentration with thermophoresis parameter N_t are shown in Fig. 11. It can be seen that the value of N_t is followed by the nanoparticle concentration profile. It occurs as a result of the increased thermophoresis force in the boundary layer area caused by a greater value of N_t , which raises the concentration of nanoparticles.

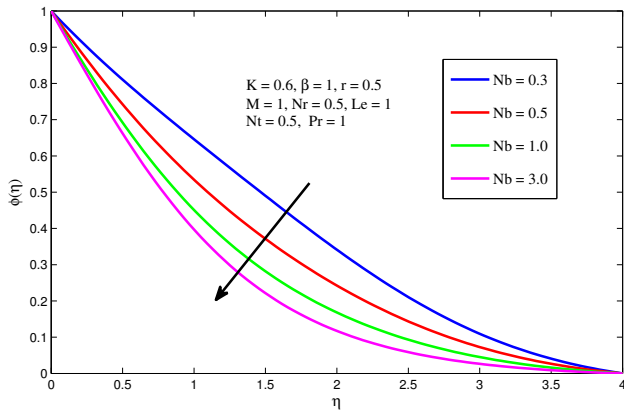


Figure 12: Effect of Brownian motion parameter on concentration profile.

Figure 12 shows the $\phi(\eta)$ for various levels of N_b . It has been shown that as N_b grows, the thermal boundary layer's thermophoresis force decreases, which lowers the boundary layer's thickness concentration. when a result, when N_b grows, the nanoparticle concentration profile decreases.

5. Conclusion

In the present investigation, the impact of thermal radiation and magnetic field on the flow of a boundary layer at the stagnation point is scrutinized. The flow occurs over a porous stretching sheet and involves a nanofluid with Casson characteristics. The governing equations are transformed into a set of differential equations without dimensions, incorporating various physical parameters. The boundary layer equations dictating momentum and heat are altered into a set of ordinary differential equations using similarity transformations. These equations are subsequently solved using the "bvp4c" function in MATLAB. The study's findings yield the following conclusions:

- An increase in the Prandtl number is associated with a reduction in thermal diffusivity, resulting in a decline in temperature.
- The skin friction coefficient is heightened by larger magnetic field parameters due to the decrease in velocity resulting from the generated Lorentz force. This decrease in velocity, in turn, leads to an increase in the drag force experienced at the surface.
- There is a drop in fluid velocity and hydrodynamic boundary layer thickness when the free-stream velocity is smaller than the stretching sheet velocity.
- The presence of a porous medium raises flow resistance, which lowers fluid motion and, as a result, lowers nanofluid velocity.
- An augmentation in thermal radiation parameter, Brownian motion parameter and thermophoresis parameter results in an augmentation in thermal boundary layer.

- This study has the potential to be applied in various areas, such as the enhancement of industrial processes like cooling systems and metal processing, the advancement of biomedical applications like drug delivery systems and the comprehension of blood flow, as well as the improvement of energy systems.

References

- [1] K. Hiemenz, Die grenzschicht an einem in den gleichformigen flüssigkeitsstrom eingetauchten geraden kreiszylinder, *Dinglers Polytech. J.* 326 (1911) 321–324.
- [2] B. Sakiadis, Boundary-layer behavior on continuous solid surfaces: Ii. the boundary layer on a continuous flat surface, *AiChE journal* 7 (2) (1961) 221–225.
- [3] F. Tsou, E. M. Sparrow, R. J. Goldstein, Flow and heat transfer in the boundary layer on a continuous moving surface, *International Journal of Heat and Mass Transfer* 10 (2) (1967) 219–235.
- [4] H. A. Ghazwani, Unsteady mixed convective mhd boundary stagnation point nanofluid flow with multi-slip effects, variable wall temperature and porosity phenomenon, *International Journal of Modern Physics B* (2023) 2450089.
- [5] A. Ali, H. S. Khan, S. Saleem, M. Hussan, Emhd nanofluid flow with radiation and variable heat flux effects along a slandering stretching sheet, *Nanomaterials* 12 (21) (2022) 3872.
- [6] V. B. Awati, A. Goravar, et al., Semi-numerical investigation of boundary layer flow and heat transfer of magnetohydrodynamics nano-fluid flow in presence of chemical reaction over a non-isothermal porous medium, *ASME Journal of Heat and Mass Transfer* 145 (8) (2023).
- [7] H. Waqas, H. Naeem, U. Manzoor, S. Sivasankaran, A. A. Alharbi, A. S. Alshomrani, T. Muhammad, Impact of electro-magneto-hydrodynamics in radiative flow of nanofluids between two rotating plates, *Alexandria Engineering Journal* 61 (12) (2022) 10307–10317.
- [8] M. Kemparaju, B. Lavanya, M. M. Nandeppanavar, N. Raveendra, Casson mhd nano fluid flow with internal heat generation and viscous dissipation of an exponential stretching sheet., *International Journal of Heat & Technology* 40 (3) (2022).
- [9] P. Thakur, A. Pargaonkar, S. S. Sonawane, Introduction to nanofluids, in: *Nanofluid Applications for Advanced Thermal Solutions*, Elsevier, 2023, pp. 1–19.
- [10] H. Song, Y. Ye, Z. Zhang, S. Wang, T. Zhou, J. Guo, S. Zhang, A nanocleaning fluid for downhole casing cleaning, *Polymers* 15 (6) (2023) 1447.
- [11] Y. Norasia, M. Tafrikan, B. H. Kamaluddin, Analysis of the magneto-hydrodynamics nanoviscous fluid based on volume fraction and thermo-physical properties, *BAREKENG: Jurnal Ilmu Matematika dan Terapan* 17 (1) (2023) 0331–0340.
- [12] G. Vanitha, U. Mahabaleswar, S. Bhattacharyya, Impact of thermal radiation on free-forced convective nanofluid flow due to a porous stretching/shrinking surface, in: *Conference on Fluid Mechanics and Fluid Power*, Springer, 2021, pp. 291–296.
- [13] B. S. Goud, Y. D. Reddy, Numerical simulation of thermal radiation on an unsteady mhd nanofluid flow over an infinite vertical flat plate with ramped temperature, *Special Topics & Reviews in Porous Media: An International Journal* 14 (2) (2023).
- [14] A. Asghar, L. A. Lund, Z. Shah, N. Vrinceanu, W. Deebani, M. Shutaywi, Effect of thermal radiation on three-dimensional magnetized rotating flow of a hybrid nanofluid, *Nanomaterials* 12 (9) (2022) 1566.
- [15] B. K. Sharma, A. Kumar, R. Gandhi, M. M. Bhatti, N. K. Mishra, Entropy generation and thermal radiation analysis of emhd jeffrey nanofluid flow: Applications in solar energy, *Nanomaterials* 13 (3) (2023) 544.
- [16] N. Vijay, K. Sharma, Entropy generation analysis in mhd hybrid nanofluid flow: Effect of thermal radiation and chemical reaction, *Numerical Heat Transfer, Part B: Fundamentals* (2023) 1–17.
- [17] H. Yasmin, Z. Nisar, Mathematical analysis of mixed convective peristaltic flow for chemically reactive casson nanofluid, *Mathematics* 11 (12) (2023) 2673.
- [18] M. Devi, U. Gupta, J. Sharma, Casson nanofluid instability with viscosity

and conductivity variation using brinkman model, *Journal of Nanofluids* 12 (4) (2023) 955–966.

[19] M. Basit, M. Tahir, A. Riasat, S. Khan, M. Imran, A. Akgül, Numerical simulation of bioconvective casson nanofluid through an exponentially permeable stretching surface, *International Journal of Modern Physics B* (2023) 2450128.

[20] M. S. Arif, K. Abodayeh, Y. Nawaz, Design of finite difference method and neural network approach for casson nanofluid flow: A computational study, *Axioms* 12 (6) (2023) 527.

[21] M. S. Arif, K. Abodayeh, Y. Nawaz, Design of finite difference method and neural network approach for casson nanofluid flow: A computational study, *Axioms* 12 (6) (2023) 527.

[22] S. Rosseland, *Astrophysik: Auf atomtheoretischer grundlage* (1931).